Classification of Activated Microglia by Convolutional Neural Networks

Chao-Hsiung Hsu
Molecular Imaging Laboratory,
Department of Radiology,
Howard University,
Washington, DC, USA
Email: chaohsiung.hsu@howard.edu

Micah Kadden
Department of Critical Care Medicine,
Children's National Hospital,
Washington, DC, USA
Email: mkadden@childrensnational.org

Yu-Shun Lin
Molecular Imaging Laboratory,
Department of Radiology,
Howard University,
Washington, DC, USA
Email: 0988516388alen@gmail.com

Michael Shoykhet
Department of Critical Care Medicine,
Children's National Hospital,
Washington, DC, USA
Email:
mshoykhet@childrensnational.org

Artur Agaronyan
Molecular Imaging Laboratory,
Department of Radiology,
Howard University,
Washington, DC, USA
Email: aagarony@umd.edu

Hoai T. Ton
Department of Critical Care Medicine,
Children's National Hospital,
Washington, DC, USA
Email: hton@childrensnational.org

Yih-Jing Lee
School of Medicine,
Fu-Jen Catholic University,
New Taipei City, Taiwan
Email: yjlee@mail.fju.edu.tw

Tsang-Wei Tu
Molecular Imaging Laboratory,
Department of Radiology,
Howard University,
Washington, DC, USA
Email: tsangwei.tu@howard.edu

Raffensperger Katherine
Department of Critical Care Medicine,
Children's National Hospital,
Washington, DC, USA
Email:
kraffenspe@childrensnational.org

Frank Wu
Molecular Imaging Laboratory,
Department of Radiology,
Howard University,
Washington, DC, USA
Email: stylefk1218@gmail.com

Paul C. Wang
Molecular Imaging Laboratory,
Department of Radiology,
Howard University,
Washington, DC, USA
Department of Physics,
Fu-Jen Catholic University,
New Taipei City, Taiwan
Email: pwang@howard.edu

2022 IEEE Biomedical Circuits and Systems Conference (BioCAS) | 978-1-6654-6917-3/22/$31.00 ©2022 IEEE | DOI: 10.1109/BioCAS54905.2022.9948635

***Abstract*—Microglia are the macrophages resident in the central nervous system. Brain injuries, such as traumatic brain injury, hypoxia, and stroke, can induce inflammatory responses accompanying microglial activation. The morphology of microglia is notably diverse and a prominent manifestation of activation. In this study, we propose to classify activated microglia using a convolutional neural network (CNN). Iba1 images were acquired from a control and cardiac arrest Long-Evans rat brain with a bright-field microscopy. The training data of 54,333 single-cell images were collected from the cortex and midbrain areas and curated by experienced neuroscientists. Results were compared between CNNs with different architectures, including Resnet18, Resnet50, Resnet101, and support vector machine classifiers. The highest model performance was found by Resnet18, trained after 120 epochs with a classification accuracy of 95.5-98.8 percent. The findings indicate a potential application for using CNN in the quantitative analysis of microglial morphology over regional differences in a large brain section.**

Keywords—microglia, cell morphology, cardiac arrest, CNN

I. Introduction

As resident macrophages in the central nervous system, microglia are activated in response to neuroinflammation in many brain diseases and injuries, such as traumatic brain injury, stroke, and hypoxic-ischemic brain injury after cardiac arrest (CA) [1]–[4]. Microglial morphology is closely related to its activation status, hence the morphological analysis of microglia has been widely used to provide quantitative indices of neuroinflammation [5]–[7]. Several machine learning and deep learning algorithms, with supervised or unsupervised data, have been used to characterize the state of microglia in various animal disease models.

Unsupervised algorithms (e.g., K-means or hierarchical clustering methods) require cell morphology parameters calculated from segmented cell images to identify the activation states of microglia [8]–[12]. On the other hand, supervised learning algorithms, such as Support Vector Machines (SVM) or Convolutional Neural Networks (CNN), require extensive manual labeling of segmented cell images [13], [14]. Silburt and Aubert [15] trained a SVM to identify activated microglia and astrocytes after focused ultrasound treatment using cellular features extracted from sliding-window on mouse brain images. However, most of the existing models are limited to detecting microglia in a relatively small region that has uniform brain structure. A few models attempt to detect region-specific microglial activation in a large field of view, but lose the resolution necessary to delineate the features in each individual cells.

In this study, we propose to utilize CNNs for the classification of activated microglia in two pathological conditions from different brain regions. The training data were prepared for individual microglia images curated from the cortex and midbrain of control and cardiac arrested rat brains. Results of residual neural networks were compared between Resnet18, Resnet50, Resnet101, and a three-convolution layer CNN (CNN3CL). We also compared the CNNs with SVM classifiers trained by raw cell images or by the features extracted from Resent18. Results show superior performance with Resnet18 trained after 120 epochs for microglia classification.

This study was supported by NIH grants of NINDS R01NS112294, R01NS123442, NCATS UL1TR001409, NICHD P50HD105328, NIMHD U54MD007597, and Howard University BFPSAP award.

II. Materials and Methods

A. Animal model and immunohistochemistry

Ischemic brain injury was induced in one-week-old Long-Evans rats by 12-minute CA surgery and compared with the non-surgical control brain [4]. All rat brains were perfused with 4% paraformaldehyde, extracted, then sectioned at 40 μm thickness. Immunohistochemistry (IHC) staining was performed with the primary ionized calcium-binding adapter (Iba1) antibody, followed by bright-field microscopy using 20X objective for taking images in 0.464 μm/pixel resolution. Slices located at ~5 mm posterior to the bregma were studied.

B. Image data sets

The locations of individual microglia were obtained by applying multiple thresholding steps on the grayscale image followed by manual corrections to fine-tune the bounding box of each cell. Each single-cell image was then resized to 120x120 pixels by zero-padding for CNNs. Classification of single-cell image data was evaluated by (1) four classes according to the pathological-regional conditions: the control cortex (Ctrl-COR), control midbrain (Ctrl-MB), CA cortex (CA-COR), and CA midbrain (CA-MB), or (2) two classes by pathological conditions: Ctrl and CA. In total, 18,524, 7,928, 18,078, and 9,803 images were taken from Ctrl-COR, Ctrl-MB, CA-COR, and CA-MB, respectively. 6,000 and 12,000 images were randomly selected in each of the four-class and two-class data sets, respectively, for training and the remainders for validation.

C. CNN and SVM

The pre-trained Resnet18, Resnet50, and Resnet101 for 1000 object categories were modified with the input image size 120x120 pixels and the number of classes in the output layer for transfer learning [16], [17]. For comparison, CNN with three convolutional layer, CNN3CL, consisted of three repeated convolution - Rectified Linear Unit (ReLu) - max-pooling layers, followed by fully connected - ReLu - fully connected layers, and a softmax layer to the output, was trained from random biases and weights [18].

All CNNs were trained by homemade Matlab programs using stochastic gradient descent with momentum (SGDM) algorithm, with the momentum = 0.9, piecewise learning rate schedule, shuffle at every epoch, and the initial learning rate was set to 0.001 for CNN3CL and 0.1 for the Residual Networks. Training times for 60 epochs (eps) were 24, 43, 143, and 292 minutes for CNN3CL, Resnet18, Resnet50, and Resnet101, respectively, using an NVIDIA GeForce RTX 2070 GPU. Resnet18(120eps) trained with additional 60 epochs, totaling 120 epochs, used 48 minutes from the previous weights. Multi-class SVM classifiers with a linear kernel were trained by a fast stochastic gradient descent solver [19] using the labeled grayscale images in SVM@images or the features extracted from Resnet18(60eps) or Resnet18(120eps) in SVM@Rsenet18.

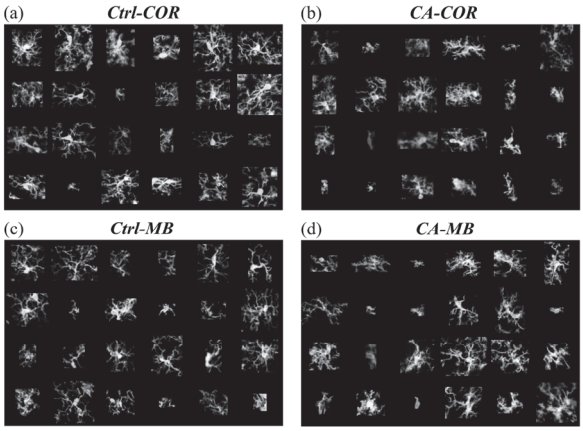

(e)

Number of Images	Four Classes			
	Ctrl-COR	*Ctrl-MB*	*CA-COR*	*CA-MB*
Training	6,000	6,000	6,000	6,000
Validation	12,524	1,928	12,078	3,803

Number of Images	Two Classes	
	Ctrl	*CA*
Training	12,000	12,000
Validation	14,452	15,881

CNNs	*Trainint Epochs*
CNN3CL	60
Resnet18	60
Resnet18	120
Resnet50	60
Resnet101	60
SVM@images	
SVM@Resnet18 Layer-Features	

Fig. 1. Groundtruth images and experimental setup. Single-microglia images were prepared from the (a) cortex of control (Ctrl-Cor), (b) cortex of cardiac arrest (CA-Cor), (c) midbrain of control (Ctrl-MB), and (d) midbrain of cardiac arrest (CA-MB) rat brains. (e) Number of images in training/validation dataset for four/two classes CNNs and SVM. (CNN3CL: CNN with three convolutional layer)

III. Results

A. Four-class classification

Activated microglia were present in the hypertrophic or amoeboid form in the inflamed brain after CA, whereas the resting microglia in the control tissue appeared to show ramified morphology [4], [20], [21]. Fig. 1 shows the single microglia images in bounding boxes from the cortex and midbrain of the control and CA brains. Instead of manual labeling of individual microglia by morphology, we created cell labels based on the pathological condition, CA or

TABLE I. Accuracy and F1 score of CNNs and SVM results

CNNs and SVM Classifiers	Four Class (Ctrl - COR/MB, CA - COR/MB)				Two classes (Ctrl and CA)			
	Training Accuracy	*Training F1*	*Validation Accuracy*	*Validation F1*	*Training Accuracy*	*Training F1*	*Validation Accuracy*	*Validation F1*
CNN3CL (60eps)	68.5%	0.69	56.7%	0.55	84.1%	0.84	77.3%	0.77
Resnet18 (60eps)	73.6%	0.74	67.7%	0.64	92.3%	0.92	79.7%	0.80
Resnet18 (120eps)	95.5-98.8%	0.96-0.99	63.5-64.0%	0.59-0.61	98.8%	0.99	78.4%	0.78
Resnet50 (60eps)	93.5%	0.94	65.1%	0.62	97.7%	0.98	78.0%	0.78
Resnet101 (60eps)	88.5%	0.89	59.4%	0.53	93.3%	0.94	79.3%	0.79
SVM@images	40.1%	0.40	26.8%	0.29	61.5%	0.62	58.1%	0.58
SVM@Resnet18 $(120eps)_{4,12}$	77.7%	0.78	63.7%	0.58	80.7%	0.81	69.7%	0.70

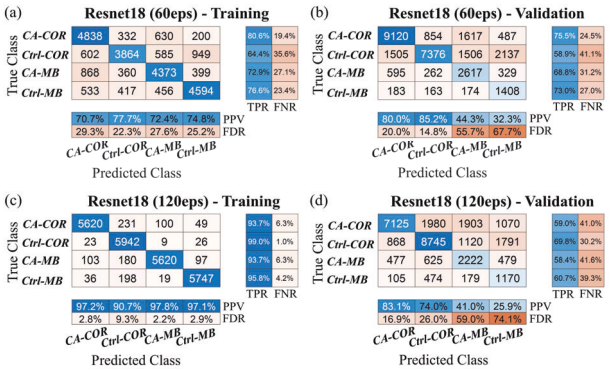

Fig. 2. Confusion matrix of four classes as shown in Figure 1. (a) Resnet18(60eps) of training, (b) Resnet18(60eps) of validation, (c) Resnet18(120eps) of training, (d) Resnet18(120eps) of validation datasets. TPR: true positive rate; FNR: false negative rate; PPV: positive predictive value; FDR: false discovery rate.

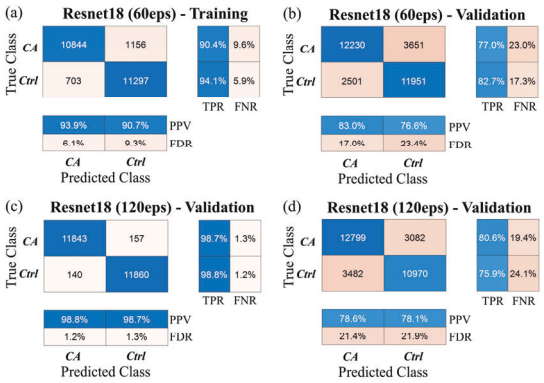

Fig. 3. Confusion matrix of two classes in control and CA brain tissues. (a) Resnet18(60eps) of training, (b) Resnet18(60eps) of validation, (c) Resnet18(120eps) of training, (d) Resnet18(120eps) of validation datasets. TPR: true positive rate; FNR: false negative rate; PPV: positive predictive value; FDR: false discovery rate.

control, and their location in the brain, cortex or midbrain. Microglia showed large diversity and morphological varieties in all four classes: Ctrl-COR, Ctrl-MB, CA-COR, and CA-MB.

Microglia in the CA brains were less branched than those in the control brains. Although the morphological differences of cells among the four classes appeared to be smaller than the differences within each class, the CNNs were able to distinguish the subtle features among the four classes. As shown in Table I, in the tests of different CNNs, the best training accuracy and F1 was 95.5-98.8% and 0.96-0.99 by Resnet18(120eps), while the best validation accuracy and F1 was 67.7% and 0.64 by Resnet18(60eps). The validation accuracies converged after about 100 epochs in Resnet18.

The training accuracy of Resnet18(120eps) was higher than that of Resnet18(60eps), yet the validation accuracies were opposite, at 63.5% vs. 67.7%. The relatively high training accuracies suggest the overfitting of CNNs. Fig. 2 illustrates the confusion matrices of the four classes from Resnet18(60eps) and Resnet18(120eps) on training and validation sets. The true positive rates (TPR) and positive predictive values (PPV) of Resnet18(120eps) were all higher than 90% in the training dataset. In contrast, Resnet18(60eps) misidentified more microglia in Ctrl-COR as Ctrl-MB, whereas microglia in CA-MB were mislabeled as CA-COR and vice versa. The difference implied that some microglia in the cortex and midbrain may have similar morphology.

B. Two-class classification

Fig. 3 and Table 1 demonstrate the results for microglia detection in two classes (Ctrl vs CA). Compared with the four-class results, both the accuracy and F1 score of the two-class CNNs improved, especially the validation accuracy increased from 56-67% to 77-79%. As shown in Fig. 3, Resnet18(60eps) and Resnet18(120eps) achieved 90% and 98% of TPR and PPV, respectively, in the training data, while they were both larger than 75% in the validation dataset. Results suggest that CNN can recognize different microglia morphology between the Ctrl and CA brain with high accuracy.

C. Prediction Images of CNNs

Fig. 4 demonstrates the images obtained from the cortex and midbrain of the control and CA brain with the bounding boxes colored in four-class ground truth labels: green for Ctrl-COR, blue for Ctrl-MB, red for CA-COR, and yellow for CA-MB. Resnet50 and Resnet101 had lower accuracy compared to Resnet18, which indicates increasing the complexity of the model has no benefit to the current dataset. Meanwhile, the underfitting of CNN3CL implied that the features between the cortex and midbrain of either control or CA brain cannot be captured accurately by only three convolutional layers (Fig. 4(b)).

D. SVM from layer features of Resnet18

The SVM classifiers were trained by the same four-class training images (Fig. 4(g)) or by the extracted features from

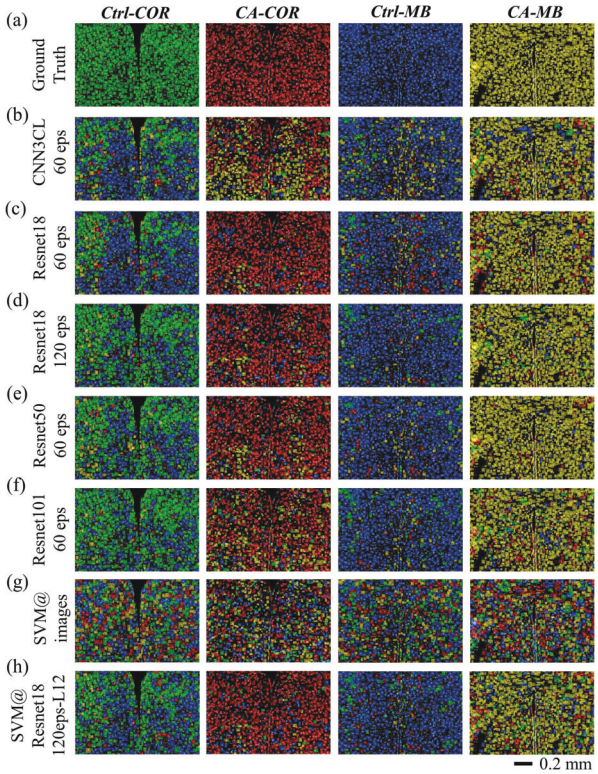

Fig. 4. Predictions of CNNs and SVMs in the cortex and midbrain. (a) Ground truth, (b) CNN3CL, (c) Resnet18(60eps) (d) Resnet18(120eps), (e) Resnet50(60eps), (f) Resnet101(60eps), (g) SVM trained from labeled images, (h) SVM from features of layer 12 of Resnet18(120eps).

Resnet18. As shown in Fig. 5(a), the accuracy of the SVM classifiers increased with the depth of the feature extraction layers. Generally, the SVM results obtained by the Resnet18(120eps) features had higher training accuracy than those obtained from the Resnet18(60eps) features after layer 20, where the accuracies reached plateau. Fig. 4(g) and 4(h) show the predicted images of the SVM classifier (SVM@images) trained by the raw images or by the features extracted from layer 12 of Resnet18 (120eps) (SVM@Resnet18(120eps-L12)). The training accuracy of SVM@images was only 40.13%, which means it was difficult to classify microglia without cell features. The results from SVM@Resnet18(120eps-L12) were similar to those of CNN3CL, because the architecture of the first 12 layers in Resnet18 also contained three convolution layers. Fig. 5(b) and 5(c) show examples of the four-class cell images and their feature maps obtained from layer 12 of Resnet18 (120eps). The high contrast of the cell body, as well as the large surrounding background area, were the major features contributing to the judgments in the CNNs and SVM.

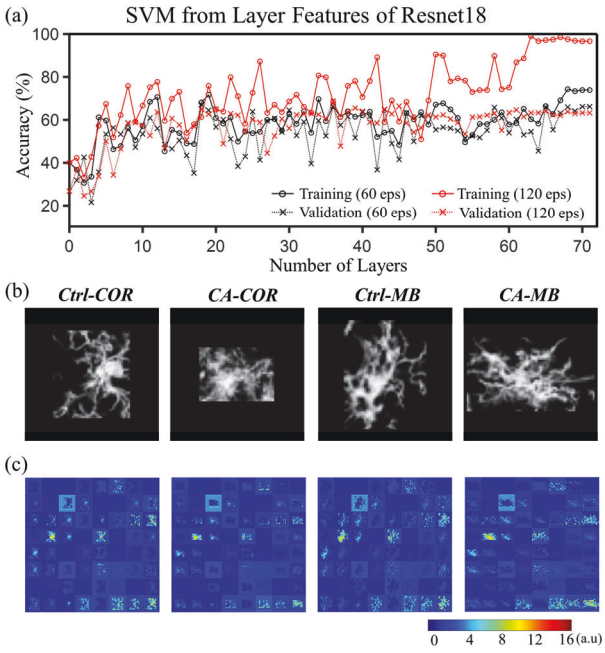

Fig. 5. Results of SVM classifier using CNN features. (a) Training and validation accuracies of SVM classifiers by features extracted from different layer of Resnet18 - 120 epochs (layer 0 denotes the raw images). (b) Images from the four classes, and (c) their 64 feature maps (size of 30x30) from layer 12 of Resnet18 - 120 epochs (a.u.: arbitrary units).

IV. Discussion

CNN and SVMs are increasingly used for biomedical image classification [1], [13]–[15], [22]–[24]. For the analysis of microglia images, most studies utilize a classification system based on the morphological phenotypes of microglia, such as ramified, hyper-ramified, activated, rod, and amoeboid morphotypes [13], [14]. In this study, CNNs were tested on identifying microglia based on a simple classification system defined by the anatomy and pathological conditions. Results showed that CNNs can accurately identify resting microglia in the control brain as well as mostly activated microglia in the CA brains, without the inputs of microglial morphotypes.

SVM was able to classify the microglia based on features extracted from segmentation results, such as cell area, cell perimeter, and cell circularity [13]. SVM performed inferiorly when trained with the cell images directly, because each image pixel was treated as an independent variable. This may result in the loss of correlation between pixels (Fig. 4(g)). When using the features extracted from Resnet18, SVM can classify microglia adequately, which demonstrates the value of feature extraction by CNNs.

In Resnet18(120eps), the SVM training accuracy increased by each "addition layer", demonstrating the advanced nature of Residual Networks. However, the validation accuracy did not increase with these residual features, suggesting that the CNN may not capture the features in the entire dataset, or cannot identify similarities among the categories. Also, the imbalance in cell number between each class in the validation set (24,602 cells from the cortex and 5,731 cells from the midbrain) may lower the validation accuracy. It is possible to prevent overfitting by adding more training data or training with data augmentation or cross-validation [25], [26]. Accordingly, SVM may be useful to understand how a CNN works by evaluating the features extracted from different CNN, therefore helping the design of a better architecture for specific datasets.

It is worthy to note that the four- or two-class ground truth that were tested in this study did not consider the fact that microglia may have the same morphotype in different regions, or even in different pathological conditions. The classification system in the tested ground truths did not reflect the actual spatial distribution of microglia by morphology in the brain tissues. Interestingly, even with the ground truths that defined microglia inaccurately, the CNNs still recognized the morphological features from the majority of microglia that were correctly defined, which were the resting microglia in the control brain, and the activated microglia in the CA brain.

CNN3CL and Resnet18(60eps) both showed that some microglia in the center cortex appeared similar to those in the midbrain (Fig. 4(b) and 4(c)). The "false" classification results by CNNs perhaps reveal that the microglia were not properly classified in the ground truth. As suggested by Fernández-Arjona's study [11], microglia should be classified by a morphometric parameter grading system in a region-specific manner. These results suggest that it may be possible to utilize CNNs, and a properly defined classification system, to create a morphological atlas by detecting the distributions of specific cell features in the brain.

The orientation of microglia is an important feature related to brain structure and the slicing direction of IHC slides. The current model may not be suitable for slides in different locations or orientations. Further study comparing the 2D projection images with 3D Z-stack images would be interesting. Furthermore, microglia morphology can vary not only by regional and pathological conditions, but also by different staining variables, slice thickness, focus, exposure and color tone, etc. More training data are required to enable CNNs to be widely applicable to analyze stained slices of varying image quality.

V. Conclusion

In this work, CNNs were demonstrated to successfully detect microglial activation in the IHC images. The CNNs can distinguish microglia between the cortex and midbrain of control and CA treated brains. The finding suggests a strong potential for CNN to perform region-specific quantification of microglia in a large brain section.

References

[1] A. D. Kyriazis, S. Noroozizadeh, A. Refaee, W. Choi, L. T. Chu, A. Bashir, W. H. Cheng, R. Zhao, D. R. Namjoshi, S. E. Salcudean, C. L. Wellington and G. Nir, "An End-to-end System for Automatic Characterization of Iba1 Immunopositive Microglia in Whole Slide Imaging," Neuroinformatics, vol. 17, no. 3, pp. 373–389, 2019.

[2] C. Kaur, G. Rathnasamy and E. A. Ling, "Roles of activated microglia in hypoxia induced neuroinflammation in the developing brain and the retina," J. Neuroimmune Pharmacol., vol. 8, no. 1, pp. 66–78, 2013.

[3] S. Heindl, B. Gesierich, C. Benakis, G. Llovera, M. Duering and A. Liesz, "Automated morphological analysis of microglia after stroke," Front. Cell. Neurosci., vol. 12, no. April, pp. 1–11, 2018.

[4] H. T. Ton, K. Raffensperger and M. Shoykhet, "Early Thalamic Injury After Resuscitation From Severe Asphyxial Cardiac Arrest in Developing Rats," Front. Cell Dev. Biol., vol. 9, no. December, pp. 1–13, 2021.

[5] J. L. Bollinger, C. M. Bergeon Burns and C. L. Wellman, "Differential effects of stress on microglial cell activation in male and female medial prefrontal cortex," Brain. Behav. Immun., vol. 52, pp. 88–97, 2016.

[6] R. Kongsui, S. B. Beynon, S. J. Johnson and F. R. Walker, "Quantitative assessment of microglial morphology and density reveals remarkable consistency in the distribution and morphology of cells within the healthy prefrontal cortex of the rat," J. Neuroinflammation, vol. 11, no. 1, pp. 1–9, 2014.

[7] H. Morrison, K. Young, M. Qureshi, R. K. Rowe and J. Lifshitz, "Quantitative microglia analyses reveal diverse morphologic responses in the rat cortex after diffuse brain injury," Sci. Rep., vol. 7, no. 1, pp. 1–12, 2017.

[8] Y. Lu, L. Carin, R. Coifman, W. Shain and B. Roysam, "Quantitative Arbor Analytics: Unsupervised Harmonic Co-Clustering of Populations of Brain Cell Arbors Based on L-Measure," Neuroinformatics, vol. 13, no. 1, pp. 47–63, 2015.

[9] F. Verdonk, P. Roux, P. Flamant, L. Fiette, F. A. Bozza, S. Simard, M. Lemaire, B. Plaud, S. L. Shorte, T. Sharshar, F. Chrétien and A. Danckaert, "Phenotypic clustering: A novel method for microglial morphology analysis," J. Neuroinflammation, vol. 13, no. 1, 2016.

[10] B. M. Davis, M. Salinas-Navarro, M. F. Cordeiro, L. Moons and L. DeGroef, "Characterizing microglia activation: A spatial statistics approach to maximize information extraction," Sci. Rep., vol. 7, no. 1, pp. 1–12, 2017.

[11] M. del M. Fernández-Arjona, J. M. Grondona, P. Granados-Durán, P. Fernández-Llebrez and M. D. López-Ávalos, "Microglia morphological categorization in a rat model of neuroinflammation by hierarchical cluster and principal components analysis," Front. Cell. Neurosci., vol. 11, no. August, pp. 1–22, 2017.

[12] L. Salamanca, N. Mechawar, K. K. Murai, R. Balling, D. S. Bouvier and A. Skupin, "MIC-MAC: An automated pipeline for high-throughput characterization and classification of three-dimensional microglia morphologies in mouse and human postmortem brain samples," Glia, vol. 67, no. 8, pp. 1496–1509, 2019.

[13] S. Choi, D. Hill, L. Guo, R. Nicholas, D. Papadopoulos and M. F. Cordeiro, "Automated characterisation of microglia in ageing mice using image processing and supervised machine learning algorithms," Sci. Rep., vol. 12, no. 1, pp. 1–12, 2022.

[14] J. Leyh, S. Paeschke, B. Mages, D. Michalski, M. Nowicki, I. Bechmann and K. Winter, "Classification of Microglial Morphological Phenotypes Using Machine Learning," Front. Cell. Neurosci., vol. 15, Jun.2021.

[15] J. Silburt and I. Aubert, "MORPHIOUS: an unsupervised machine learning workflow to detect the activation of microglia and astrocytes," J. Neuroinflammation, vol. 19, no. 1, pp. 1–20, 2022.

[16] "ImageNet." [Online]. Available: http://www.image-net.org.

[17] H. Kaiming, X. Zhang and J. Ren, Shaoqing, Sun, "Deep residual learning for image recognition," Proc. IEEE Conf. Comput. Vis. pattern Recognit., pp. 770–778, 2016.

[18] MathWorks, "Train Object Detector Using R-CNN Deep Learning," Matlab, 2019.

[19] J. Donahue, Y. Jia, O. Vinyals, J. Hoffman, N. Zhang, E. Tzeng and T. Darrell, "DeCAF: A deep convolutional activation feature for generic visual recognition," 31st Int. Conf. Mach. Learn. ICML 2014, vol. 2, pp. 988–996, 2014.

[20] K. Helmut, U. K. Hanisch, M. Noda and A. Verkhratsky, "Physiology of microglia," Physiol. Rev., vol. 91, no. 2, pp. 461–553, 2011.

[21] A. Ousta, L. Piao, Y. H. Fang, A. Vera, T. Nallamothu, A. J. Garcia and W. W. Sharp, "Microglial Activation and Neurological Outcomes in a Murine Model of Cardiac Arrest," Neurocrit. Care, vol. 36, no. 1, pp. 61–70, 2022.

[22] D. Maric, J. Jahanipour, X. R. Li, A. Singh, A. Mobiny, H. VanNguyen, A. Sedlock, K. Grama and B. Roysam, "Whole-brain tissue mapping toolkit using large-scale highly multiplexed immunofluorescence imaging and deep neural networks," Nat. Commun., vol. 12, no. 1, pp. 1–12, 2021.

[23] Y. Ding, M. C. Pardon, A. Agostini, H. Faas, J. Duan, W. O. C. Ward, F. Easton, D. Auer and L. Bai, "Novel Methods for Microglia Segmentation, Feature Extraction, and Classification," IEEE/ACM Trans. Comput. Biol. Bioinforma., vol. 14, no. 6, pp. 1366−1377, 2017.

[24] M. Liu, J. Ylanko, E. Weekman, T. Beckett, D. Andrews and J. McLaurin, "Utilizing supervised machine learning to identify microglia and astrocytes in situ: implications for large-scale image analysis and quantification," J. Neurosci. Methods, vol. 328, no. August, p. 108424, 2019.

[25] J. D. Domingo, R. M. Aparicio and L. M. G. Rodrigo, "Cross Validation Voting for Improving CNN Classification in Grocery Products," IEEE Access, vol. 10, pp. 20913–20925, 2022.

[26] P. Thanapol, K. Lavangnananda, P. Bouvry, F. Pinel and F. Leprevost, "Reducing Overfitting and Improving Generalization in Training Convolutional Neural Network (CNN) under Limited Sample Sizes in Image Recognition," InCIT 2020 - 5th Int. Conf. Inf. Technol., pp. 300–305, 2020.

[27] M. Young, The Technical Writer's Handbook. Mill Valley, CA: University Science, 1989.